Characterization of Microstructure and Mechanical Properties of Biodegradable Polymer Blends of Poly(L-lactic acid) and Poly(butylene succinate-*co*-ϵ-caprolactone) With Lysine triisocyanate

Vilay Vannaladsaysy,[1,2] Mitsugu Todo,[1] Mariatti Jaafar,[2] Zulkifli Ahmad,[2] Korakanh Pasomsouk[3]

[1] *Research Institute for Applied Mechanics, Division of Fundamental Mechanics, Kyushu University, Kasuga, Fukuoka, Japan*

[2] *School of Materials and Mineral Resources Engineering, Universiti Sains Malaysia, Nibong Tebal 14300, Pulau Pinang, Malaysia*

[3] *Department of Mechanical Engineering, Faculty of Engineering, National University of Laos, Vientiane, Laos*

Effect of lysine triisocyanate (LTI) as an additive on the microstructure and the mechanical properties of biodegradable polymer blends of poly(L-lactic acid) (PLLA) and poly(butylene succinate-*co*-ε-caprolactone) (PBSC) were investigated by using Fourier transform infrared (FTIR) spectroscopy, differential scanning calorimetry (DSC), field-emission scanning electron microscope (FE-SEM), and bending and mode I fracture testing techniques. It was found that the addition of LTI dramatically improves the phase-separation morphology of the PLLA/PBSC blends. FTIR analysis suggested that the NCO groups of LTI were acted as compatibilizer by attributing secondary process between the two polymers PLLA and PBSC, resulting lower peak intensity of ACI samples, understood as secondary process is polar interaction and hydrophobic process. DSC and FE-SEM results also supported such improvement of immiscibility between PLLA and PBSC. Macroscopic mechanical properties such as the bending fracture energy and the mode I fracture properties are also effectively improved by the LTI addition. Void formation is suppressed due to such morphological change in PLLA/PBSC/LTI blends, and, as a result, energy dissipation in the notch-tip region of the blends becomes higher than in that of PLLA/PBSC where localized stress concentration due to voids tends to accelerate fracture initiation and, therefore, lowers the fracture energy. POLYM. ENG. SCI., 50:1485–1491, 2010. © 2010 Society of Plastics Engineers

INTRODUCTION

Poly(L-lactic acid) (PLLA), a typical biodegradable polymer made from bioresources, has extensively been used in many industrial fields such as automotive, electrical, and medical industries. PLLA has some potential advantages such as environmental degradability and biocompatibility and also strength and modulus comparable to those of commercially available engineering polymers. In the medical industry, PLLA also has great potential of applications as bioabsorbable medical devices such as bone fixation plates, screws, and rods used in orthopedic and oral surgeries [1–3]. However, PLLA exhibits brittle fracture behavior, especially, under impact loading conditions and, therefore, the toughening of PLLA becomes one of the most important issues in the field of biopolymer engineering [4]. Several approaches have been used to improve the mechanical properties of PLLA, for example, blending with a ductile biodegradable polymer is known to be an effective way [5–20]. The common ductile biodegradable polymers used in such PLLA blending are poly(ε-caprolactone) (PCL) [8, 17, 18], poly(butylene succinate) (PBS) [13, 15, 20], poly(butylene succinate-*co*-L-lactate) (PBSL) [13, 14, 20], and poly(butylene succinate-*co*-ε-caprolactone) (PBSC) [19, 20]. It is known that in general these PLLA polymer blends exhibit phase-separation morphology, e.g., secondary polymers are dispersed in PLLA matrix when the polymers are directly blended without any additives [20]. Just recently, it was found that addition of lysine triisocyanate (LTI) can effectively improve the immiscibility in PLLA/PCL, PLLA/PBS, and PLLA/PBSL blends, and, as a result, their mechanical properties become higher [15–19]. However, effects of LTI addition on PLLA/PBSC blend have not been clarified yet.

The objective of this study was therefore to characterize the effects of LTI addition on the microstructures and

Correspondence to: Mitsugu Todo; e-mail: todo@riam.kyushu-u.ac.jp
DOI 10.1002/pen.21683
Published online in Wiley InterScience (www.interscience.wiley.com).

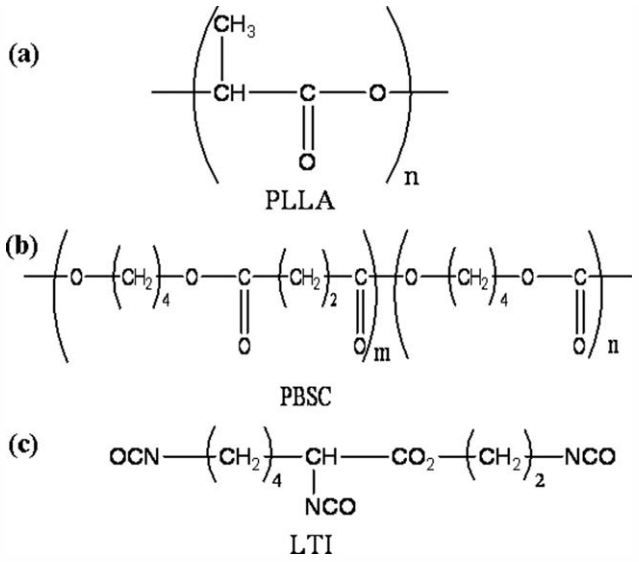

FIG. 1. Chemical structures of the base polymers: (a) PLLA, (b) PBSC, and (c) LTI.

the mechanical properties of PLLA/PBSC blend. Differential scanning calorimetry (DSC), Fourier transform infrared (FTIR) analyses, and scanning electron microscopy (SEM) of cryofractured surfaces were performed to characterize the microstructural modification generated in the blend due to LTI addition. Mode I fracture and three-point bending tests were also carried out to assess the change appeared in the mechanical properties. These macroscopic properties were then correlated with the microscopic structural modification.

EXPERIMENTAL

Materials and Specimens

PLLA pellets ($M_w = 1.45 \times 10^5$) and PBSC pellets ($M_w = 1.7 \times 10^5$) were supplied by Toyota Motor Co. and Daicel Chemical Industries, respectively. These pellets were held into a desiccator to keep them dry and to prevent them from degradation because of hydrolysis by moisture. High viscous solution of LTI was supplied by Kyowa Co. The chemical structures of PLLA, PBSC, and LTI are shown in Fig. 1. Blends of PLLA and PBSC, with and without addition of LTI, were prepared by melt-mixing in a conventional melt-mixer at 190°C and at a rotor speed of 50 rpm for 20 min. Blend ratios of PLLA and PBSC were chosen to be 90/10, 80/20, and 70/30 in weight fraction, and the amount of LTI mixed with the blends was fixed to be 2 phr. The mixtures were then compression molded at 30 MPa for 190°C, and then followed by cooling process using a water cooling system to produce sheets of $140 \times 140 \times 2$ mm^3. Sheets of neat PLLA were also fabricated through the same molding process. Bend specimens and single-edge-notch-bend (SENB) specimens for mode I fracture tests were then prepared from these sheets. The dimensions of both testing samples were approximately $50 \times 10 \times 2$ mm^3. Table 1 exhibits the sample labeling with corresponding compositions.

FTIR and DSC Measurements

FTIR measurements were carried out using Bio-Rad FTS-6000 spectrometer with resolution of 8 cm^{-1} for 32 scans over wave number range of 400–4000 cm^{-1}. The samples were obtained by casting films of polymer resolution on the KBr disc. The solvent (chloroform) was evaporated at room temperature for at least 5 min before recording the IR spectra.

DSC analysis was conducted using DSC-60 installed with TA-60WS thermal analysis system (Shimadzu Co.). Approximately 8–10 mg samples were weighted and put into an aluminum pan with a cover. The samples were scanned from −100 to 230°C at a scan rate of 10°C/min under nitrogen atmosphere to determine the thermal property of the samples. The melting temperature, T_m, and the glass transition temperature, T_g, of the neat polymers and the blends were then evaluated from the DSC curves, and the intrinsic degree of crystallinity, $X_{c\ PLLA}$, was also determined based on the following formula:

$$X_{c\ PLLA}(\%) = \frac{(\Delta H_c - \Delta H_m) \times 100}{93 \times X_{PLLA}} \quad (1)$$

where ΔH_c and ΔH_m are the enthalpies of crystallization and melting of PLLA, respectively, and the constant of 93 J/g is the fusion enthalpy of PLLA [8]. X_{PLLA} is the weight fraction of PLLA.

Mechanical Tests

Three-point bending tests of the beam specimens were performed at a load-rate of 1 mm/min using a servo-hydraulic testing machine. Load-displacement relations were recorded using a digital recorder. For all testing measurements, at least five specimens were tested to obtain the average and standard deviation (SD). The ultimate bending strength and the flexural modulus were then determined using the following formulae:

TABLE 1. Sample designation and composition of materials.

Sample code	Composition	Weight percent (wt%)
PLLA	PLLA	100
PBSC	PBSC	100
AC_{10}	PLLA/PBSC	90/10
ACI_{10}	PLLA/PBSL/LTI	90/10/2
AC_{20}	PLLA/PBSC	80/20
ACI_{20}	PLLA/PBSC/LTI	80/20/2
AC_{30}	PLLA/PBSC	70/30
ACI_{30}	PLLA/PBSC/LTI	70/30/2

 DOI 10.1002/pen

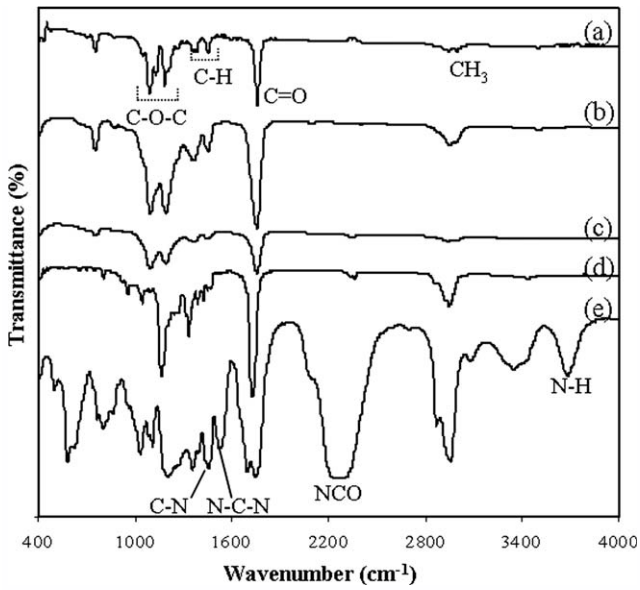

FIG. 2. FTIR spectra: (a) PLLA, (b) AC_{20}, (c) ACI_{20}, (d) PBSC, and (e) LTI.

$$\sigma_f = \frac{3PL}{2bh^2} \text{ and } E = \frac{L^3}{4bh^3}S \tag{2}$$

where P is the maximum load. S is the slope of the initial linear portion of the load-displacement curve. L, b, and h are the span length, width, and the thickness, respectively.

Mode I fracture tests of the SENB specimens were performed at a loading-rate of 1 mm/min by using the servo-hydraulic testing machine. Load-displacement relations were recorded using the digital recorder. Mode I fracture properties such as the initial fracture energy, J_{in}, which is defined as the critical J-integral value at crack initiation, and the averaged fracture energy, J_f, were then evaluated using the following formulae:

$$J_{in} = \frac{\eta U_{in}}{B(W-a)} \tag{3}$$

$$J_f = \frac{U_f}{B(W-a)} \tag{4}$$

where U_{in} is the critical energy at crack initiation that is defined as the point where the stiffness of the specimen starts to rapidly decrease. U_f is the total fracture energy that is dissipated by the complete fracture of the specimen. B and W are the specimen thickness and width, respectively, a is the initial crack length and η the geometrical correction factor, where $\eta = 2$ for the standard SENB specimen.

FE-SEM Observations

Cryo-fracture surfaces were obtained by immersing the specimens into liquid nitrogen for 30 min. The surfaces were then observed using a field emission SEM (FE-SEM; HITACHI S-4100) to characterize microstructural morphology. Fractured surfaces of the SENB specimens were also observed by FE-SEM to characterize microscopic deformation mechanisms and effect of LTI addition on the fracture behavior.

RESULTS AND DISCUSSION

FTIR Results

Figure 2 shows the FTIR spectra of PLLA, PBSC, LTI, AC_{20}, and ACI_{20}. It is seen that PLLA, PBSC, and the blends exhibited very similar spectra patterns with the C=O peak at about 1700 cm^{-1}. However, the C=O peak of PBSC (d) was much higher than that of PLLA (a). It is, therefore, understood that the higher C=O peak of AC_{20} (b) than PLLA was a result of PBSC blending. It is clearly seen that the C=O peak of ACI_{20} (c) became lower than that of AC_{20}, suggesting that the mobility of PLLA and PBSC molecules reduced due to LTI addition. On the other hand, the spectra of LTI (e) were obviously characterized by the existence of the large NCO peak around 2200 cm^{-1}. It is noted that there was no apparent peak of NCO in the spectra of ACI_{20}, indicating that NCO groups acted as compatibilizer by attributing secondary process between the two polymers PLLA and PBSC. This secondary process is polar interaction and hydrophobic process.

The best way to analyze the FTIR data based on these propositions would be to compare the spectra of AC_{20} and ACI_{20} (refer to Fig. 3). Based on FTIR analysis, the peak responding to C = O group appeared higher peak intensity for the sample without the addition of LTI. This refers to difference in bonding motion between that of PLLA and PBSC. However, after addition of LTI, these peaks shift lower, which indicate an identical bond motion in carbonyl group between the two copolymers. This can be attributed to the effect of the LTI, which

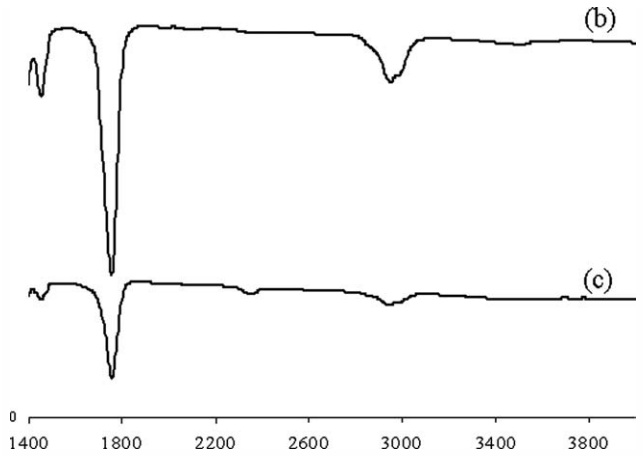

FIG. 3. Comparison of FTIR spectra of AC_{20} (b) and ACI_{20} (c).

formed good polar interaction between both PLLA and PBSC. This interaction induces the mobilities of the respective carbonyl bonds as unit entity. This is in agreement with the previous works that showed changes in peak shift and intensity as the results interchange of interaction because of the secondary process [21, 22].

DSC Results

Figure 4 shows the DSC curves for heating thermograms of neat PLLA, PBSC, AC_{20}, and ACI_{20}. Points corresponding to the crystallization temperature (T_c), the melting temperature (T_m), and the glass transition temperature (T_g) are also shown in Fig. 4. The values of T_c, T_m, T_g, and the degree of crystallinity of PLLA are summarized in Table 2. In the neat PLLA thermogram (a), the heat jump at about 64°C corresponded to T_g, followed by the melting peak at about 177°C. On the other hand, the thermogram of the neat PBSC reveals that its T_m occurred at about 105°C and T_g was found at −42.8°C, although the heat jump was not clearly seen in this thermogram. According to previous work [23], the syntheses of PBSC with different CL/BL ratios show melting and glass transition temperatures ranging between 39 to 107°C and −38 to −58°C, respectively, to be illustrating PBSC in this research.

For the thermogram of AC_{20}, it is obvious that the T_m peaks of PLLA and PBSC and the heat jump at T_g of PLLA still exist and, furthermore, T_g of PBSC was also defined. Two exothermic peaks existed in the AC_{20} thermogram, the former appearing at 90°C was attributed to the typical cold crystallization of PLLA, and the second appearing just before the melting point of PLLA could be explained by the possibility of recrystallization of lower perfection crystals of polylactide into α crystal of the higher perfection [24]. For the thermogram of ACI_{20}, it is noted that the isothermic peaks corresponding to T_m and T_g of PBSC were totally disappeared, indicating that the immissibility between PLLA and PBSC was effectively improved because of LTI addition, so that PBSC molecules could not freely be moved.

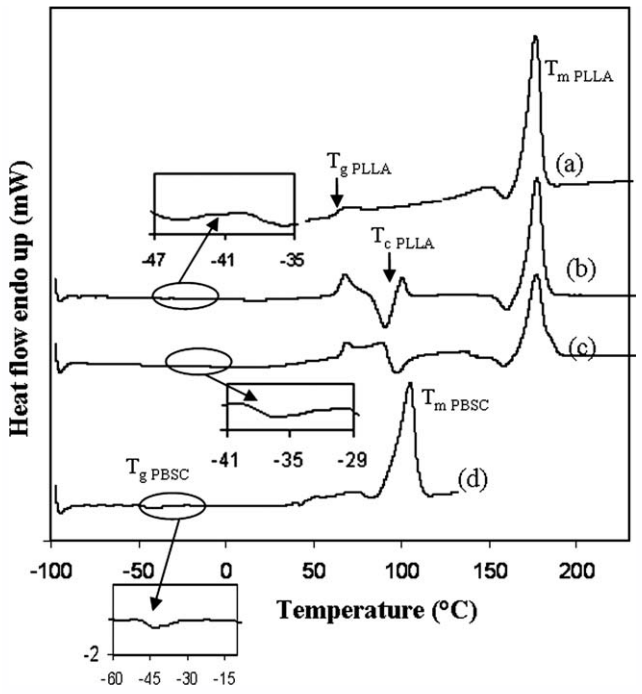

FIG. 4. DSC thermograms: (a) PLLA, (b) AC_{20}, (c) ACI_{20}, and (d) PBSC.

TABLE 2. Thermal properties of neat PLLA, PBSC, and the blends.

	PLLA			PBSC		
Materials	T_g (°C)	T_m (°C)	T_c (°C)	T_g (°C)	T_m (°C)	$X_{c\ PLLA}$ (%)
PLLA	64.44	177.09	—	—	—	—
PBSC	—	—	—	−44.14	105.13	—
AC_{10}	63.24	174.44	88.66	−42.9	98.25	68.98
ACI_{10}	62.95	173.86	95.18	−40.24	—	73.67
AC_{20}	63.65	177.25	90.78	−40.1	100.47	59.54
ACI_{20}	62.88	177.1	97.36	−35.71	—	40.07
AC_{30}	63.68	176.59	89.69	−42.18	99.89	58.99
ACI_{30}	62.08	176.48	97.79	−32.49	—	43.79

The levels of crystallinity, X_c, of the blends are shown in Table 2. It is clearly seen that the blends of PLLA/PBSC with and without LTI possessed the crystallinity values, whereas the neat PLLA exhibited almost amorphous state corresponding to no apparent crystallization peak. For the blends, it is obvious that ACI showed lower crystallinity than AC because of the improvement of immiscibility.

Microstructural Morphology

FE-SEM micrographs of the cryo-fractured surfaces are shown in Fig. 5. Evolution of spherulitic morphology appeared on all of PLLA/PBSC blends. The spherical structures constructed the secondary phase and, therefore, corresponded to PBSC spherulites. It is apparent that the spherical structures became large with increasing PBSC content. This kind of morphological result agrees with immiscible polymer blends that generally create macrophase separation of the two components due to difference of solubility parameter [3]. Such phase separation usually affects the physical and mechanical properties of the blend [25]. On the contrary, for PLLA/PBSC blends with LTI, apparent circular structures of PBSC could not be observed on the surfaces. This is due to improvement of miscibility between PLLA and PBSC. Such microstructural improvement is understood to be caused by the chemical reaction between NCO and OH groups as discussed based on the FTIR results given in the previous section.

Mechanical Properties

Bending mechanical properties are listed in Table 3. The bending strength decreased due to blending with

 DOI 10.1002/pen

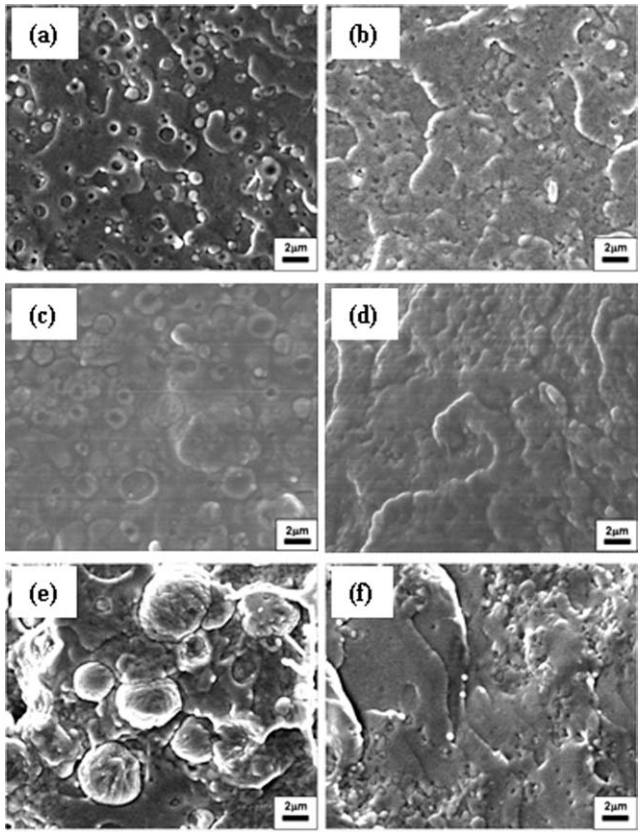

FIG. 5. FE-SEM micrographs of microstructures: (a) AC_{10}, (b) ACI_{10}, (c) AC_{20}, (d) ACI_{20}, (e) AC_{30}, and (f) ACI_{30}.

PBSC having much lower strength than PLLA. It is clearly shown that LTI addition improved the strength of the blends. Effects of blending and LTI addition on the flexural modulus were very similar to those on the strength. The total fracture energy values dissipated during bending deformation are also shown in Table 3. Blending and LTI addition tended to improve the bending energy; however, the energy of ACI_{30} was lower than that of PLLA and the other blends, because effect of the ductile secondary PBSC phase on the bending deformation became significant.

Typical load-displacement curves obtained from the mode I fracture tests are shown in Fig. 6. In general, the maximum load almost coincides with the onset of crack growth in the tip of notch introduced. It is, therefore,

TABLE 3. Bending properties of neat PLLA, PBSC, and the blends.

Materials	Strength (MPa)	Modulus (GPa)	Energy (kJ/m^2)
PLLA	99.62 ± 7.1	3.99 ± 0.35	21.5 ± 0.2
PBSC	32.1 ± 1.1	0.71 ± 0.18	6.6 ± 0.7
AC_{10}	91.98 ± 2.62	3.56 ± 0.1	22.72 ± 1.1
ACI_{10}	92.3 ± 6.6	3.91 ± 0.26	24.06 ± 2.2
AC_{20}	90.7 ± 6.3	3.29 ± 0.2	21.31 ± 2.2
ACI_{20}	94.21 ± 4.7	3.72 ± 0.12	23.88 ± 1.23
AC_{30}	73.94 ± 4.9	2.56 ± 0.3	12.8 ± 3.7
ACI_{30}	84.8 ± 1.7	3.73 ± 0.17	20.7 ± 0.8

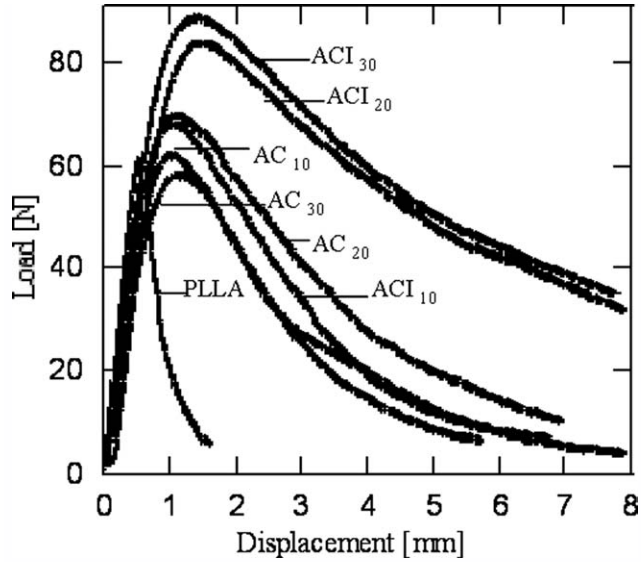

FIG. 6. Load-displacement curves obtained from the mode I fracture tests.

understood that the much higher maximum load of ACI_{20} and ACI_{30} indicated dramatic improvement of resistibility to crack initiation. The slope of the load-displacement curve after the maximum load usually corresponds to the rate of crack growth. Therefore, the much gentler slopes of the blends indicated slower crack growth than the rapid growth in PLLA characterized by a steep slope.

Effects of LTI addition on the initial fracture energy, J_{in}, and the averaged fractured energy, J_f, are shown in Fig. 7. It is seen that J_{in} of PLLA/PBSC blends were slightly higher than that of neat PLLA; on the contrary, J_{in} of PLLA/PBSC/LTI increased with increase of PBSC content, and J_{in} of ACI_{30} was about three times larger than that of neat PLLA. J_f values of AC blends were higher than that of PLLA, and the improvement of J_f due to blending reached its peak at 20 wt% of PBSC. On the contrary, J_f of ACI effectively increased with increase of PBSC content, and J_f of ACI_{30} was about seven times larger than that of PLLA. These experimental results clearly exhibited that LTI addition effectively improved the mode I fracture properties such as J_{in} and J_f of PLLA/PBSC polymer blends.

Fracture Surface Morphology

FE-SEM micrographs of fracture surfaces in the note-tip regions are shown in Fig. 8. It is apparent that PLLA created a flat and smooth surface compared to the rough fracture surfaces of PLLA/PBSC blends. The blends showed plastic deformation behavior characterized by elongated fibril structures. It is also seen that the surfaces of PLLA/PBSC, characterized by the existence of many voids, are much rougher than those of PLLA/PBSC/LTI. It is naturally understood that these voids were created by removal of the PBSC spherulites shown in Fig. 5. The

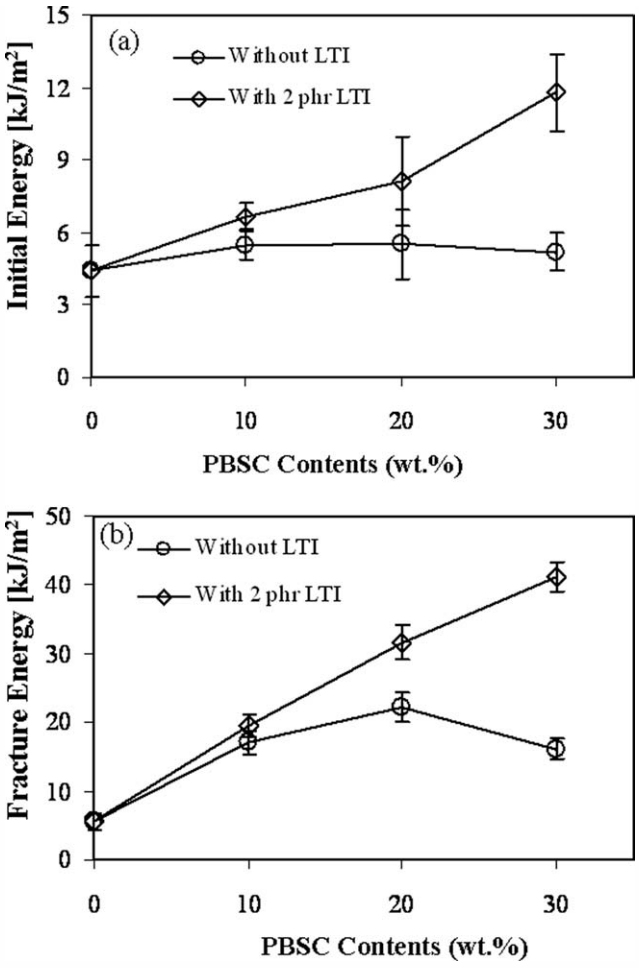

FIG. 7. Effect of PBSC content and LTI addition on the fracture energy values: (a) Initial fracture energy, J_{in}, and (b) averaged fracture energy, J_f.

size of the spherulites tended to increase with increasing PBSC content as shown in Fig. 6 and, therefore, the size of the voids also increased as PBSC content increased. It is noted that the voids were created due to debonding at the interfaces between the spherulites and the matrix under a low stress level, because of the lower interfacial strength than the strength of the base polymer. The crystallization, i.e., the spherulite formation process of PBSC takes place at a lower temperature than the crystallization process of PLLA and, therefore, the PBSC spherulites cannot firmly connect with the surrounding PLLA matrix at the interfaces. It is easily understood that the voids cause localized stress concentration in the surrounding matrix and, therefore, accelerates fracture initiation in the notch-tip region. Larger spherulites correspond to wider interfacial regions and also stronger interactions between the spherulites, and, therefore, faster the interfacial failure and lower the fracture energy as shown in Fig. 6. When LTI was added to the mixture of PLLA and PBSC, the isocyanate groups of LTI tried to create chemical bonding with the hydroxyl groups of PLLA and PBSC, known as the urethane bonding, and, therefore, the PLLA molecules were firmly entangled with the PBSC molecules. As a result, the immiscibility of the polymers and, therefore, the fracture energy values were dramatically improved.

CONCLUSIONS

Effects of LTI addition on polymer blends of PLLA and PBSC results significant improvement in mode I fracture and bending properties of the blends. On the fracture surfaces of PLLA/PBSC blends, many voids were observed, on the contrary, for PLLA/PBSC/LTI blends, void formation was suppressed due to increase of entanglement of PLLA and PBSC molecules caused by chemical reaction. This kind of morphology change due to LTI addition resulted in the dramatic improvement of the mode I fracture properties. FE-SEM observation also showed that for PLLA/PBSC blends with LTI, apparent circular structures of PBSC that were spherulites, could

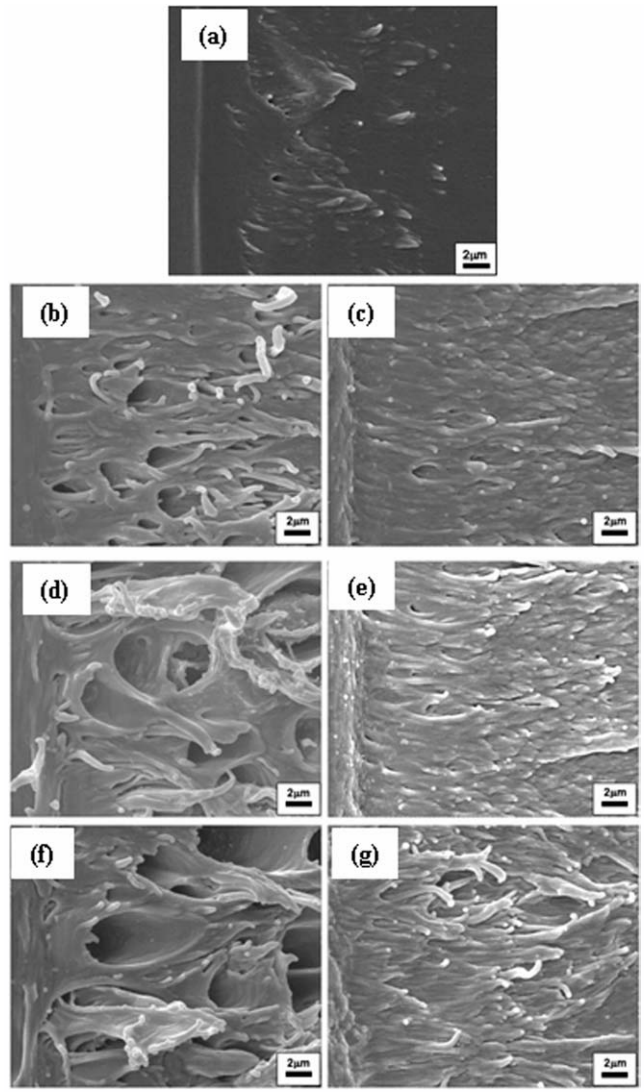

FIG. 8. FE-SEM micrographs of mode I fractured surfaces in the notch-tip regions. (a) PLLA, (b) AC_{10}, (c) ACI_{10}, (d) AC_{20}, (e) ACI_{20}, (f) AC_{30}, and (g) ACI_{30}.

 DOI 10.1002/pen

not be observed on the cryo-fractured surfaces. This corresponded to the improvement of immiscibility between PLLA and PBSC due to LTI addition. DSC curves exhibited that the isothermic peaks corresponding to T_m and T_g of PBSC were totally disappeared in PLLA/PBSCLTI blends, indicating that the immiscibility between PLLA and PBSC was effectively improved due to LTI addition, so that the PBSC molecules could not freely be moved. FTIR results suggested that the NCO groups of LTI were acted as compatibilizer by attributing secondary process between the two polymers PLLA and PBSC. It is thus suggested that LTI worked as a compatibilizer connecting between PLLA and PBSC molecules.

REFERENCES

1. S.R. Bhattarai, N. Bhattarai, H.K. Yi, P.H. Hwang, D.I. Cha, and H.Y. Kim, *Biomaterials*, **25**, 2595 (2004).
2. O.M. Bostman, *J. Bone Joint Surg*., **73-A**, 148 (1991).
3. J.W. Leenslag, A.J. Pennings, R.R.M. Bos, F.R. Rozema, and J. Boering, *Biomaterials*, **8**, 70 (1987).
4. M. Todo, S.D. Park, T. Takayama, and K. Arakawa, *Eng. Fract. Mech*., **74**, 1872 (2007).
5. A.J. Domb, *J. Polym. Sci. Part A: Polym. Chem*., **31**, 1973 (1993).
6. M. Hiljanen-Vainio, P. Varpomaa, J. Seppälä, and P. Törmälä, *Macromol. Chem. Phys*., **197**, 1503 (1996).
7. L. Wang, W. Ma, R.A. Gross, and S.P. McCarthy, *Polym. Degrad. Stab*. **59**, 161 (1998).
8. H. Tsuji, A. Mizuno, and Y. Ikada, *J. Appl. Polym. Sci*., **70**, 2259 (1998).
9. Y. Yuan and E. Ruckenstein, *Polym. Bull*., **40**, 485 (1998).
10. R. Dell'Erba, G. Groeninckx, G. Maglio, M. Malinconico, and A. Migliozzi, *Polymer*, **42**, 7831 (2001).
11. X. Cao, A. Mohamed, S.H. Gordon, J.L. Willett, and D.J. Sessa, *Thermochim. Acta*, **406**, 115 (2003).
12. K.S. Anderson, S.H. Lim, and M.A. Hillmyer, *J. Appl. Polym. Sci*., **89**, 3757 (2003).
13. M. Shibata, Y. Inoue, and M. Miyoshi, *Polymer*, **47**, 3557 (2006).
14. M. Shibata, N. Teramoto, and Y. Inoue, *Polymer*, **48**, 2768 (2007).
15. M. Harada, T. Ohya, K. Iida, H. Hayashi, K. Hirano, and H. Fukuda, *J. Appl. Polym. Sci*., **106**, 1813 (2007).
16. M. Harada, K. Iida, K. Okamoto, H. Hayashi, and K. Hirano, *Polym. Eng. Sci*., **48**, 1359 (2008).
17. T. Takayama and M. Todo, *J. Mater. Sci*., **41**, 4989 (2006).
18. T. Takayama, M. Todo, H. Tsuji, and K. Arakawa, *J. Mater. Sci*., **41**, 6501 (2006).
19. V. Vannaladsaysy, M. Todo, T. Takayama, M. Jaafar, Z. Ahmad, and K. Pasomsouk, *J. Mater. Sci*., **11**, 3006 (2009).
20. M. Todo, A. Harada, and H. Tsuji, CD-ROM, *Proc. 16th Int. Conf. Compos. Mater*., July 8–13, TuGM1–07, Kyoto, Japan (2007).
21. J. Dong and Y. Ozaki, *Macromolecules*, **30**, 286 (1997).
22. O.R. Pardini and J.I. Amalvy, *J. Appl. Polym. Sci*., **107**, 1207 (2008).
23. A. Cao, T. Okamura, C. Ishiguro, K. Nakayama, Y. Inoue, and T. Masuda, *Polymer*, **43**, 671 (2002).
24. J. Zhang, Y. Duan, H. Sato, H. Tsuji, I. Noda, S. Yan, and Y. Ozaki, *Macromolecules*, **38**, 8012 (2005).
25. H. Tsuji, *Biomaterials*, **24**, 537 (2003).